Carbon Nanotubes as a Pulsed Electron Sources

Xianqi Wei

Additional information is available at the end of the chapter

Abstract

One of the most promising applications of carbon nanotubes (CNTs) is the emission electronics, in which CNTs are used as a field emission electron source. Lots of electronic devices are based on electron sources, which are the most important components served as state-of-art nanoelectronics devices in nowadays, such as field emission displays, miniature mass spectrometers, scanning ultrafast electron microscopes, X-ray generators, free electron lasers, THz sources, and so on. Field electron emission is based on the physical phenomenon of quantum tunneling, in which electrons are emitted from the surface of materials into vacuum on the condition of applied voltage. CNTs have many advantages as field emitters comparing with conventional metallic emitters like familiar examples of tungsten, gold, copper, and molybdenum. Electron emission from cold cathodes of CNTs has attracted attentions of numerous scientists, and substantial researches have been conducted on their properties and applications. In this chapter, we will focus on the field emission of CNT cold cathodes as an electron source, including of how to synthesize it by chemical vapor deposition (CVD) method and how to realize its electron emission. In addition, we will report pulsed electron emission of CNT cathodes. The combination of the laser pulse and the cold cathode will offer the possibility of pulsed field emission. Our approach demonstrates the growth mechanism and the emission mechanism of CNTs, which is beneficial for controlling the performance of its fascinating application on emerging fields.

Keywords: carbon nanotubes (CNTs), cathodes, field emission, laser, pulse

1. Introduction

Electron field emission (or field emission for short), is a tunnel effect of electron induced by high electric field at the surface of a solid material. A distinct advantage is that no extra energy is needed for the electron tunneling process. One of the most promising applications of the field emission is an electron source. Lots of electronic devices are based on electron

sources, which are the most crucial component served as state-of-art vacuum nanoelectronics and emerging novel devices in nowadays, such as field emission displays, emerging sensor, energy storage equipment, scanning ultrafast electron microscopes, X-ray generators, free electron lasers (FELs), THz sources, and so on [1–3].

With the advent of electron beam from nanometer-scale field emitters induced by femtosecond laser, electron sources are gradually replaced by ultrafast pulsed electron sources. These sources could potentially output extremely high emission current in a very short time, providing sufficient brightness, high-energy density, high frequency (up to optical frequency), and ultrashort coherent electron bunches [4–6]. Recently, such electron sources have intrigued a strong interest and encouraged the further studies of pulsed electron emission, opening the door to high-tech novel devices. For example, pulsed electron emission opens a way toward the time-resolved electron microscopy, because electrical gating and source control enable time resolution down to picoseconds, while using optical control enables creation of electron pulses with duration down to tens of femtoseconds. Such dense and short electron bunches can become a popular platform for material and device imaging, inspection, and failure analysis. They would enable exciting technological developments like four-dimensional (4D) time resolved electron microscopy, spectroscopy, holography, single-electron sources, and carrier envelope phase detection [7, 8]. Besides, pulsed electron sources are also becoming a hot topic in fields of medicine, physics, chemistry, industry, and communication, both in military and domestic industries.

In the past few decades, metallic nanotips have been considered an attractive and popular candidate as emitters of field emission cold cathodes, such as W, Mo, Au, Cu, Co, and so on. However, it is certainly worth considering that the complicated process of manufacture and thermal ablation of metallic nanotips result in poor thermal stability and mechanical properties for practical application. Besides, metallic tips suffer from serious thermal effect in pulsed field emission, because of illuminating metallic emitters for a long time by induced laser. Moreover, with the development of technology, the main trend of new generation electronic devices faces a great challenge on limitations of high power, high frequency, and compact small size. Conventional metallic emitters cannot satisfy the higher requirements of emerging devices, which have to provide high-energy density and pulsed emission electric current [9]. High-performance field emitters with adequate excellent emission properties are highly desired. To extend the studies on conventional metallic nanotips, this paper studies the pulsed electron emitters in a popular material of CNTs.

Since the discovery by Iijima in 1991, CNTs have received more and more research interests. One of the most popular studies is about the intriguing explorations of the high-performance field emitter as an emission electron source due to the CNTs' extraordinary instinct properties of high aspect ratio, good electrical conductivity, excellent thermal conductivity, robust chemical and mechanical properties. CNTs have been considered promising field emission candidates since they were first demonstrated as electron field emitters in 1995 [10–12]. These years, considerable researches have been conducted on their useful properties, as well as synthesis methods and various applications [13]. Here, we mainly introduce the property and application about the field emission of CNTs, which are synthesized by high temperature catalytic chemical vapor deposition (CVD) method.

2. Growth of CNTs

2.1. Carbon nanotube arrays (CNT arrays)

The growth of CNT arrays follows a high temperature catalytic chemical vapor deposition (for short CVD) with iron phthalocyanine ($FeC_{32}N_8H_{16}$). In the growth process, the phthalocyanines act as not only a carbon source but also as a metallic catalyst. The growth temperature is 800–900°C for 15 min. The flow rate of hydrogen and argon are 25 and 60 sccm, respectively. The prepared CNT arrays are multi-walled nanotubes with the height of 6–10 μm and the diameter of 20–100 nm, as shown in **Figure 1**. The densely packed CNTs grow on the surface of the Si substrate. The roots stand vertically on the substrate surface and the tips entangles with each other. Detailed structures of CNT arrays are characterized by TEM as shown in **Figure 1(c)**. The synthesized CNT arrays are multi-walled nanotubes, and the interlayer spacing is about 0.34 nm, which is close to the (002) crystal plane of graphite. Besides, Raman Spectroscopy is employed to perform the Raman pattern of CNT arrays as shown in **Figure 1(d)**. Two of the sharp peaks are present at 1350 and 1350 cm⁻¹, respectively, corresponding to the disorder-induced D band and the tangential mode G band of the main Raman feature of multi-walled CNTs. Moreover, the ratio of intensities of the D and G bands, which is less than one indicates a high quantity of structure defects. And, the second-order 2D band, which is caused by the double resonant Raman scattering with two-phonon emissions, appears at 2700 cm⁻¹ [4, 14].
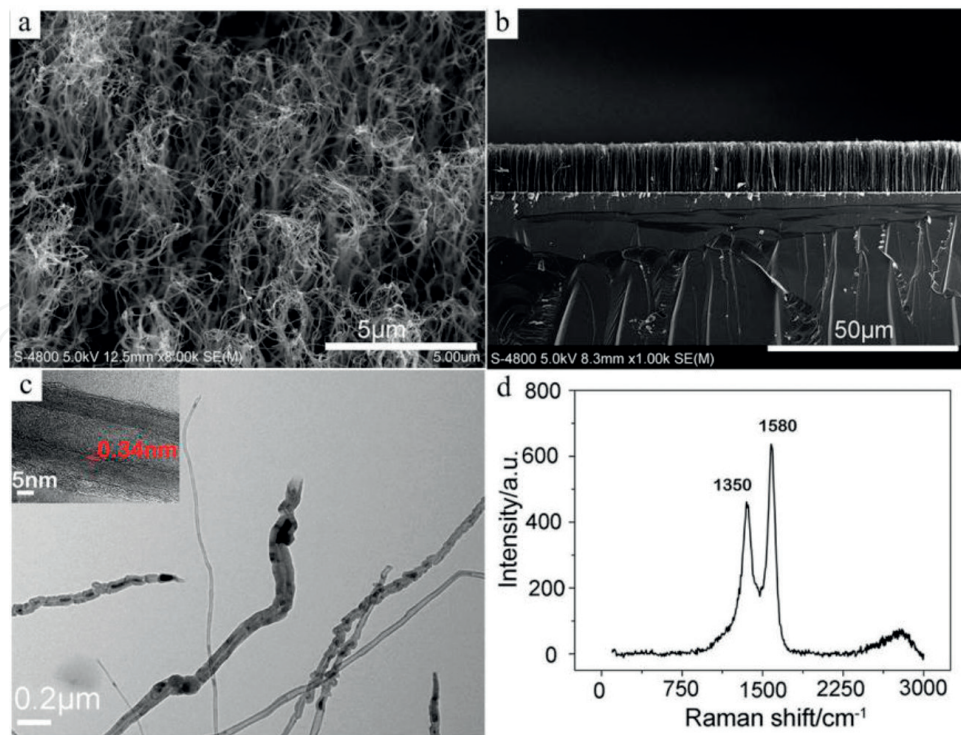

Figure 1. CNT arrays. (a) Top view, (b) sectional view, (c) TEM, (d) Raman spectrum.

2.2. Carbon nanotubes arrays-graphene composite (CNTs-G)

CNTs have been considered as a promising emitter because of their unique properties. For example, the electrical conductivity is about 10^5 S/cm and thermal conductivity is 3500 W/mK, which is better than that of many metallic emitters [15, 16]. Graphene, a desired electrical and thermal transport medium with two-dimensional sp^2 hybridized carbon atoms, is potential for field emission because of its remarkable electronic, mechanical, and thermal properties. However, the CNTs emitters are commonly attached onto the electrode surface to form the CNTs cathodes, resulting in a large contact resistance and unstable emission current. Graphene, a transparent cathode, have to design a special structure for field emission. The field emission still faces great challenges on stability and thermal effect, especially in pulsed field emission. In this part, we report the composite of CNTs-G to improve the electric and thermal transport as an emitter.

2.2.1. Bottom-up structure of the CNTs-G composite

CNTs-G composite grows by the same method as CNT arrays but the different parameters of gas flow rate. The reducing gas of hydrogen is 10 sccm and protective gas of argon is 60 sccm, respectively. The composite of CNTs-G consists of graphene sheets and CNT arrays. Graphene sheets is on the top surface and CNT arrays is on the bottom attached on the substrate surface, as shown in **Figure 2**. Graphene sheets and CNT arrays combine together tightly and form a three-dimensional (3D) cathode, which is completely different from the
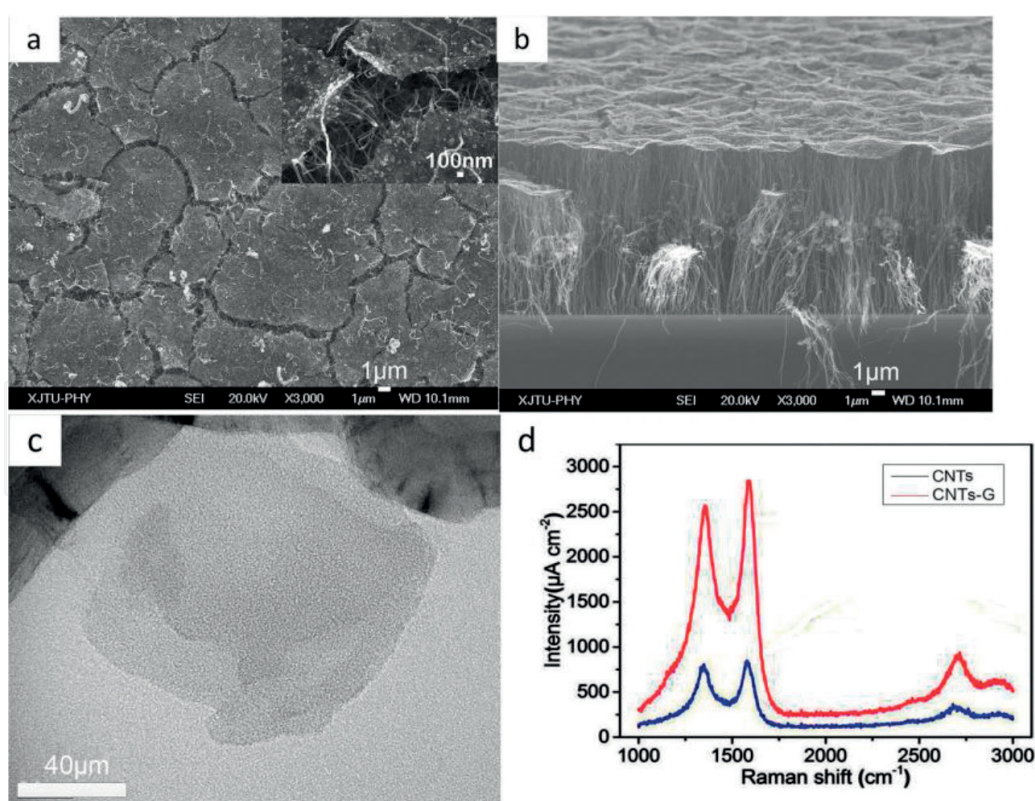

Figure 2. The composite of carbon nanotube arrays-graphene (CNTs-G). (a) Top view, (b) sectional view, (c) TEM, (d) Raman spectrum.

CNTs/graphene composite fabricated by transfer technology. The interaction between CNTs and graphene is mainly due to the Van der Waals force for the CNTs/graphene composite. Here, the 3D CNTs-G composite is directly synthesized, which is quite different from physical contact of the CNTs/graphene composite between the interface of CNTs and graphene. The 3D composite, having the vertically CNT arrays and the outstanding graphene, could provide a good electrical and thermal contact and exhibits a high performance as a thermal interface material.

The graphene sheets on the top surface of the CNTs-G composite are characterized by TEM, as shown in **Figure 2(c)**, and the composite shows a typical peak of 2D band at 2700 cm^{-1} in comparison with CNT arrays, as shown in **Figure 2(d)**. To obtain more detailed information on the chemical composition and surface electronic state of the CNTs-G composite, the X-ray photoelectron spectroscopy (XPS) examination is implemented, as shown in **Figure 3**. It can be clearly observed that Fe, O, N, and C elements exist in the spectrum. The elements of Fe and N arise from the carbon source of iron phthalocyanine ($FeC_{32}N_8H_{16}$). And, a sharp peak for C1s at 284.8 eV is observed to evaluate the binding behavior of the elements in the CNTs-G composite, which is ascribed to the graphitic carbon [17, 18].

2.2.2. Top-down structure of the CNTs-G composite

The principle of field emission is based on the application of a very high electric field to extract electrons from a metal or a highly doped semiconducting surface. However, if the field emission cathode surface has a high point or a protrusion, electrons may be extracted at
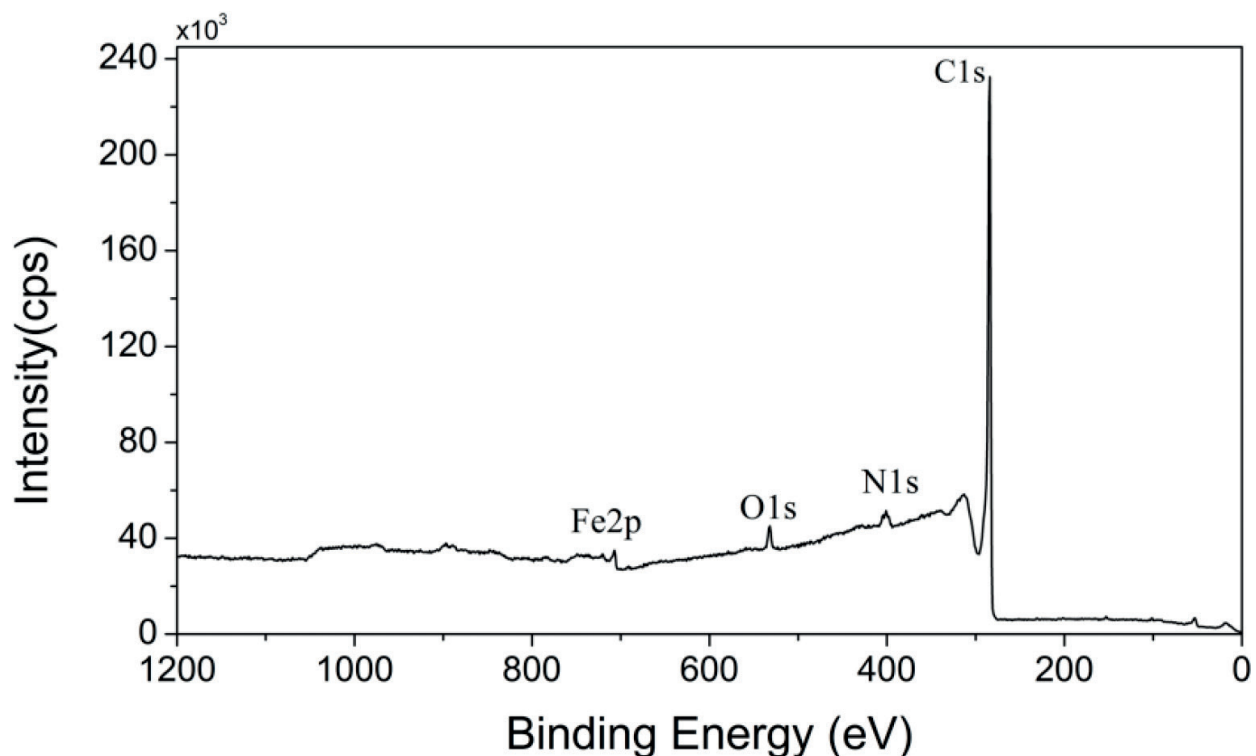

Figure 3. The full survey spectrum XPS spectra of the CNTs-G composite.

a considerably lower applied gap field. This is because the lines of force converge at the sharp point and the physical geometry of the tip provides a field enhancement [3]. So, it is desired a composite of CNTs-G, which is a top-down 3D structure. That is, CNT arrays are on the top surface of graphene, and it is tightly attached on the substrate surface as an electrode. This 3D CNTs-G composite is different from the above in the part (i). Graphene films are on the bottom grown on the substrate and CNT arrays are on the top surface, as shown in **Figure 4**. This composite was found by accident, when grew patterned CNT arrays.

From the EDX analysis shown in **Figure 4(d)**, it indicates that the composite mainly consists of C, Fe, and Si elements. The element of Fe results from the iron phthalocyanine ($FeC_{32}N_8H_{16}$), and the Si results from the substrate. Raman spectrum is carried out to further determine the structure information, as shown in **Figure 4(c)**. In comparison with CNT arrays, the Raman spectrum of films on the substrate have a typical peak at 2700 cm^{-1}, which is in accord with the 2D peak of graphene. The ratio of 2D peak height/G peak height indicates the films are
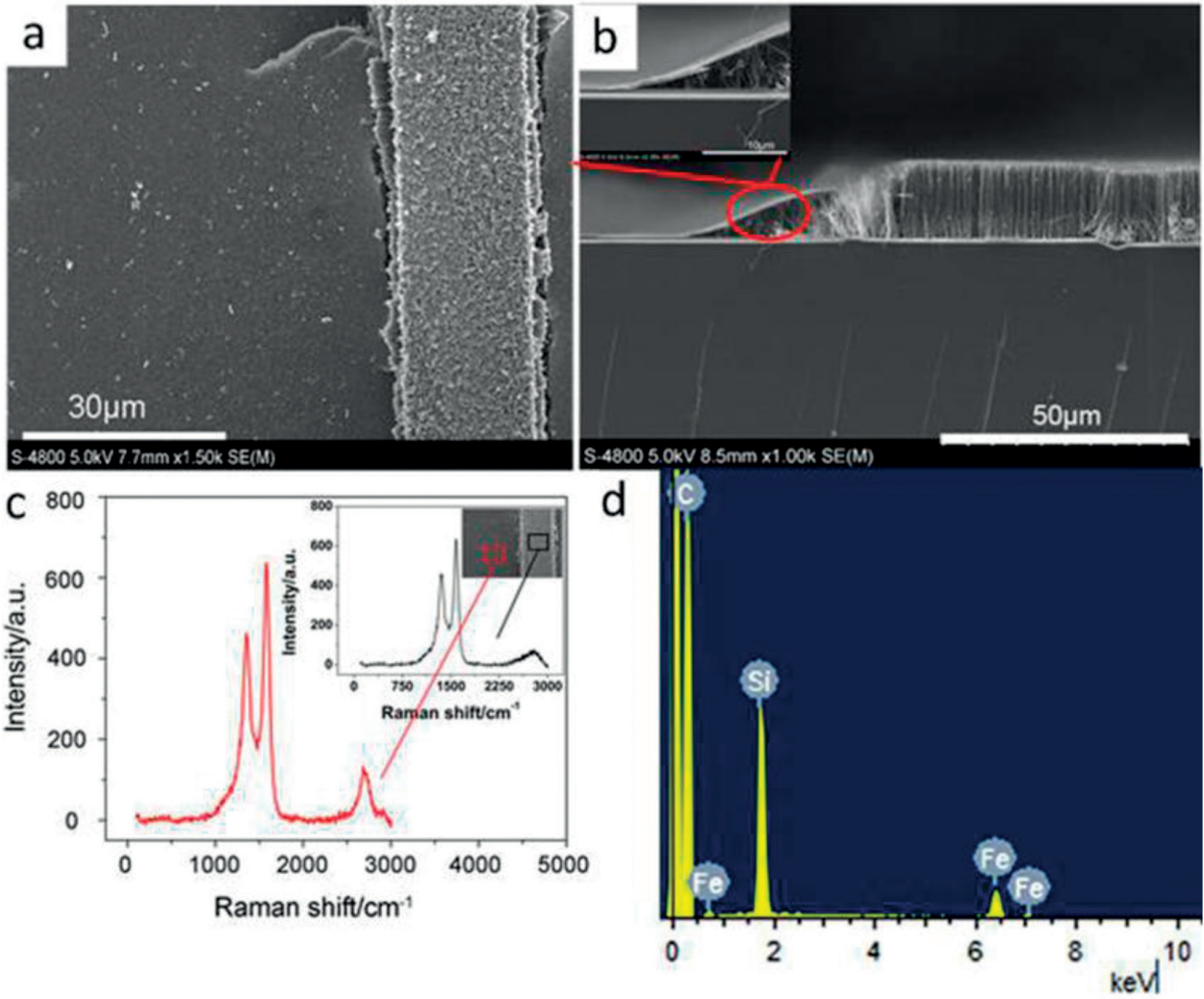

Figure 4. The top-down structure of CNTs-G composite. (a) Top view of a ribbon of CNT arrays; (b) cross sectional view; (c) Raman spectrum; (d) EDX analysis.

the multilayer graphene films. Due to the CNT arrays as field emitters and high electrical and thermal conductive of graphene films as electrode, the composite could provide a good electrical and thermal contact and exhibits a high-performance field emission.

3. Field emission

The phenomenon of the field emission is associated with a quantum mechanical tunneling process whereby electrons tunnel through a potential barrier under the influence of a high electric field. The field emission characteristic is usually described by F-N theory, given by:

$$\ln\left(\frac{J}{V^2}\right) = \ln A - \frac{B}{V} \tag{1}$$

where $A = 1.54 \times 10^{-6} S \frac{\beta^2}{\varphi}$ and $B = \frac{-6.83 \times 10^7 \varphi^{3/2} d}{\beta}$, S is the effective area of field emitters, β is the field enhancement factor, φ is the work function of field emitters, d is the distance of anode–cathode [3, 19]. Generally, it was used to improve the field emission properties by enhancing β. The sharp tips or small radius curvature of the emitter apex gives a high local electric field enhancement. In the past few years, to improve β of CNTs, novel composites of CNTs/graphene hybrids, three-dimensional CNTs and plasma treatment of CNTs have been reported to explore optimized CNTs emitters. In this part, we will introduce a cylindrical structure of CNT arrays cathodes. The morphology of CNT arrays on cylindrical substrate can be controlled by tuning the size of the substrate diameter. The work function φ of CNT arrays is supposed to 4.89 eV in this paper [20].

3.1. Planar structure

The area of CNT arrays grown on the flat substrate of Si is about 1.7 cm × 1.8 cm. The field emission measurement is carried out using diode parallel plate in vacuum 5 × 10⁻⁵ Pa. The anode–cathode spacing is 400 μm. The experimental set-up is shown in **Figure 5(a)**. **Figure 5(b)** gives the current density versus voltage (*J-V*) curves. The turn-on voltage is about 700 V (defined as the applied voltage required to generate an emission current density of 1 mA/cm²). The insert of top left in **Figure 5(b)** is Fowler-Nordheim (F-N) plots corresponding to *J-V* curves, and the bottom right is the picture of current emission on 1500 V. The F-N curve follows the linear relationship, confirming that the detected current is in agreement with field emission mechanism.

3.2. Cylindrical structure

In the previous research, CNTs were synthesized on a flat substrate such as Si, SiO$_2$, and Au. Nevertheless, we present a method to synthesize CNT arrays on cylindrical waveguide of the optical fiber substrate. CNT arrays are synthesized on the fiber surface by CVD using a same method as reported the above. The substrate is commercial quartz optical fiber with a diameter of 220 μm. To prepare fiber substrate before CNTs growth, the polymer coating
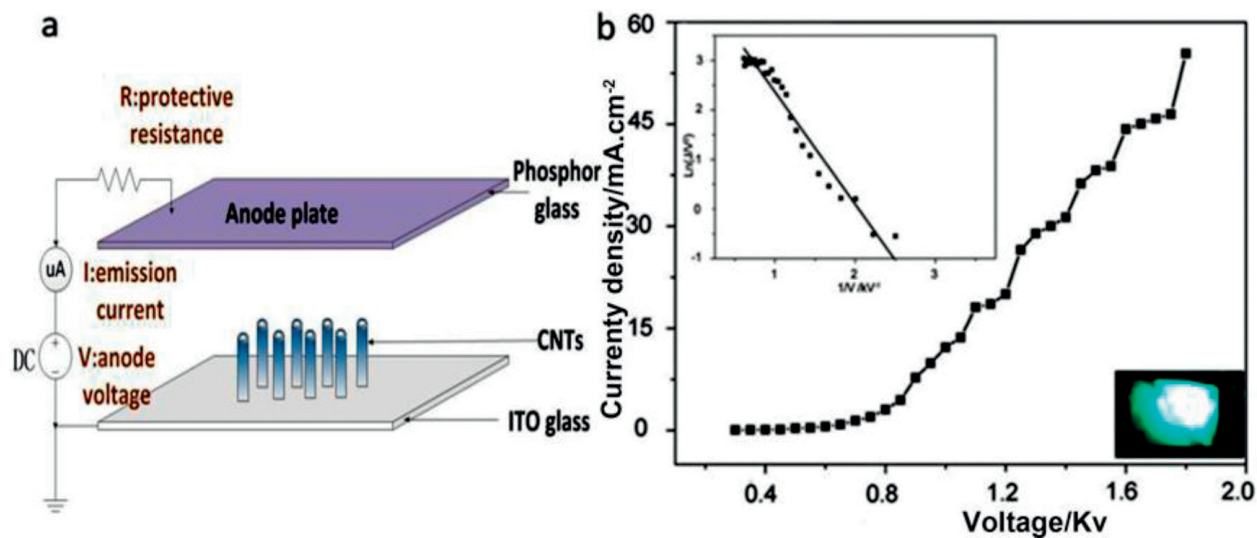
Figure 5. The field emission of the CNT arrays on Si substrate. (a) Structure diagram of experimental set-up, (b) measurement results of the field emission.

layer should be removed. Then, quartz optical fiber is corroded in dilute hydrofluoric acid (~13 wt.% HF) to the desired size by controlling the corrosion time. After treatment, the prepared fiber is used as substrate for the growth of CNT arrays.

The microstructures and morphologies of the products are characterized by SEM, TEM, and Raman spectroscopy. **Figure 6(a)** is an overall view, showing the densely packed CNT arrays covered on the fiber surface. Detailed structures of CNT arrays are characterized by TEM. **Figure 6(b)** and **(c)** are the low-magnification and high-resolution TEM image. The synthesized CNT arrays are multi-walled nanotubes with the diameters of 20–100 nm. As shown in **Figure 7(c)**, the interlayer spacing is about 0.34 nm, which is close to the (002) crystal plane of graphite. Besides, Raman pattern of CNT arrays is showed in **Figure 6(d)**. The D band appears at 1352 cm^{-1}, G band appears
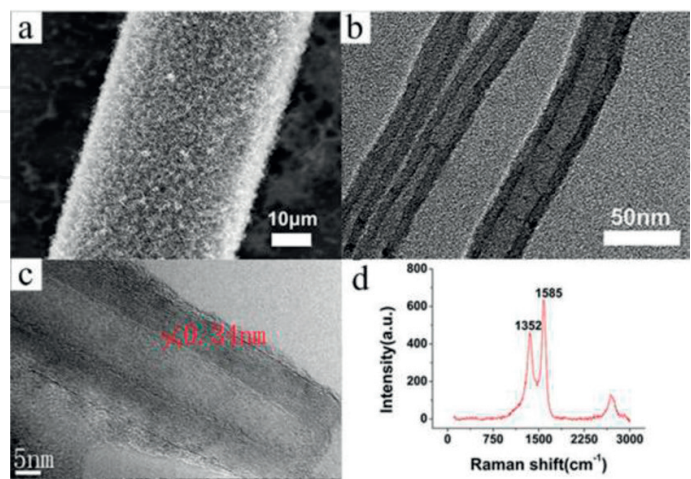

Figure 6. The scanning electron micrograph (SEM) image of CNT arrays covered on the surface of fiber substrate. (a) a overall view, (b) a low-magnification TEM image of CNTs, and (c) a high-resolution TEM image of a CNT. (d) the Raman spectrum of CNT arrays.
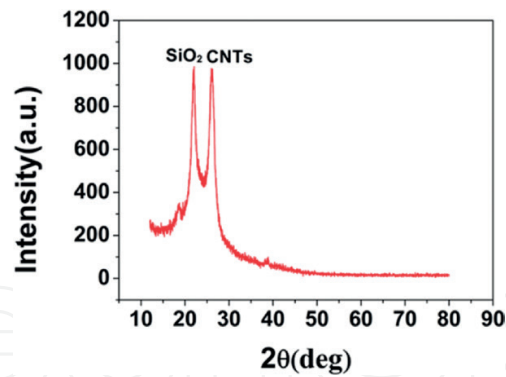
Figure 7. The X-ray diffraction pattern of CNT arrays covered on the quartz fiber surface.

at 1585 cm⁻¹, and 2D band appears at 2700 cm⁻¹, which is in agreement with the typical Raman feature of multi-walled CNTs [4, 14]. To further characterize the detailed information of the CNT arrays covered on the surface of fiber substrate, the X-ray diffractometer is employed to analyze. As shown in Figure 7, the XRD pattern of CNT arrays on fiber substrate exhibits a sharp (002) Bragg reflection at about $2\theta = 26.2°$, which is derived from the ordered arrangement of the concentric cylinders of graphitic carbon. And the peak centered on $2\theta = 21.9°$ shows the SiO_2 resulting from the quartz fiber substrate. **Figure 8(a)** is a cross-section SEM image of CNT arrays covered on the fiber substrate. CNT arrays vertically stand on the fiber surface with the uniform length and roots density. **Figure 8(c)** is a zoom in image of the CNTs roots marked in **Figure 8(a)**. The dense roots are highly aligned and vertically stand on fiber surface. The surface morphology of the CNTs
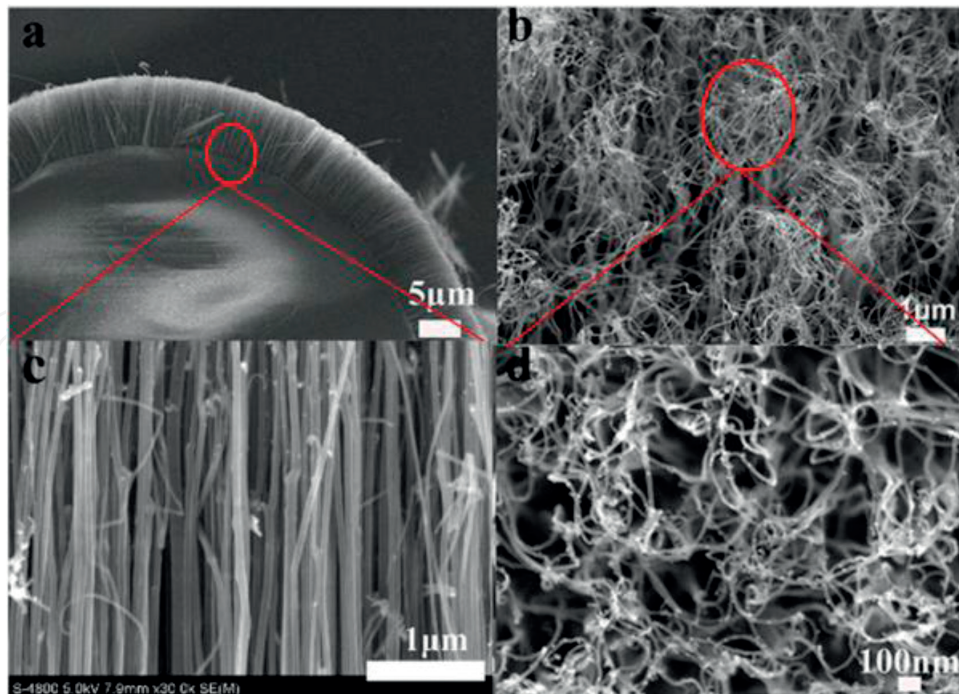

Figure 8. The SEM images of CNT arrays synthesized on the fiber substrate with the diameter of 200 μm, (a) the cross-section SEM image, (b) the top view SEM image of the surface morphology, (c) a zoomed in view of the roots, (d) a zoomed in top view of the tips.

tips are showed in **Figure 8(b)**, and a magnified top view image shows in **Figure 8(d)**. Though the dense roots of CNT arrays vertically attach on the fiber surface, the tips radiate outward dispersedly along the radial direction of fiber substrate [14]. With the fiber diameter decreased, the gaps between the CNT arrays tips are obviously distinct. And for that, the change of fiber diameter will greatly affect the tips morphology of CNT arrays, which cover on the cylindrical surface of optical fiber substrate. Decreasing the fiber diameter, the gaps between CNT tips will enlarge. The distance between the neighboring CNT arrays tips is greatly dependent on the fiber substrate, which could be changed by simply tuning the fiber diameter, as shown in **Figure 9**. **Figure 9(a), (b)** is the overall view of CNT arrays covered on the surface of fibers with diameters of 200 and 20 μm. It is noticeable that remarkable cracks on fiber substrate with diameter of 20 μm, because the tips gap of nanotubes is large on a smaller diameter curve surface. **Figure 9(c)** is a cross-section image of CNT arrays covered on the cylindrical surface of 200 μm diameter fiber, and **Figure 9(d)** is CNT arrays on the surface of fiber with a smaller diameter of 20 μm [14]. **Figure 10** gives the field emission measurement results of CNT arrays covered on fiber substrates with diameters of 200, 100, 40, 30, and 20 μm. **Figure 10(a)** is the *J-V* curves. For the fiber substrate with the diameter of 20 μm, the CNTs cathode performs the minimum turn-on voltage V_{to} (the applied voltage requires to generate an emission current density of 1 mA/cm²), yielding the maximum emission current at a low applied voltage than the others. When the diameter of fiber substrate decreases from 200 to 20 μm, the turn-on voltage V_{to} obviously decreases and the emission current density increased at the same applied voltage. β of the CNT arrays increases from 7823 to 11,631, and the turn-on voltage V_{to} decreases from 1290 to 109 V, corresponding to the data as shown in **Table 1**.

It is a well-known fact that β of nano cathodes has a significant effect on field emission properties. This is because the local electric field on the sharp emitters resulting in a field enhancement, which is expressed as β. However, there is a screening effect on the top tips of emitters, because of close spacing on dense individual tips. Screening effect weaken
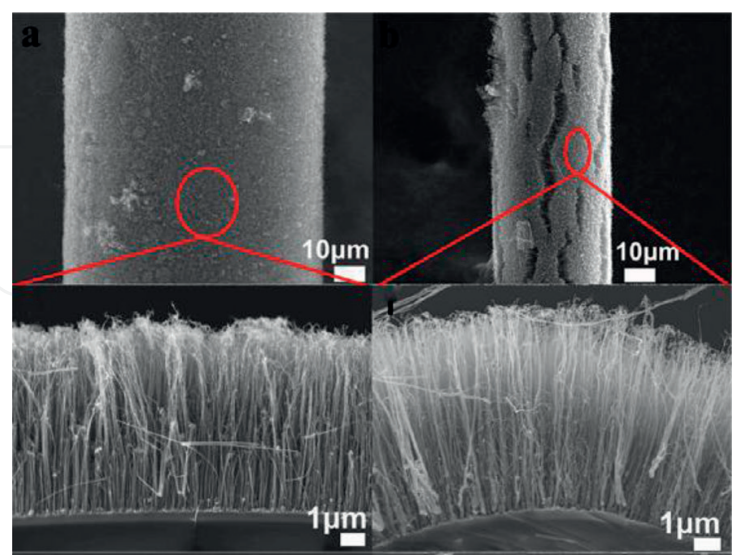

Figure 9. (a) The overall view of CNT arrays on fiber surfaces with diameters of 200 μm; (b) overall view of CNT arrays on fiber surface with diameter of 20 μm; (c) and (d) are cross-section images of CNT arrays on the surface of fiber substrate with the diameter of 200 and 20 μm, respectively.
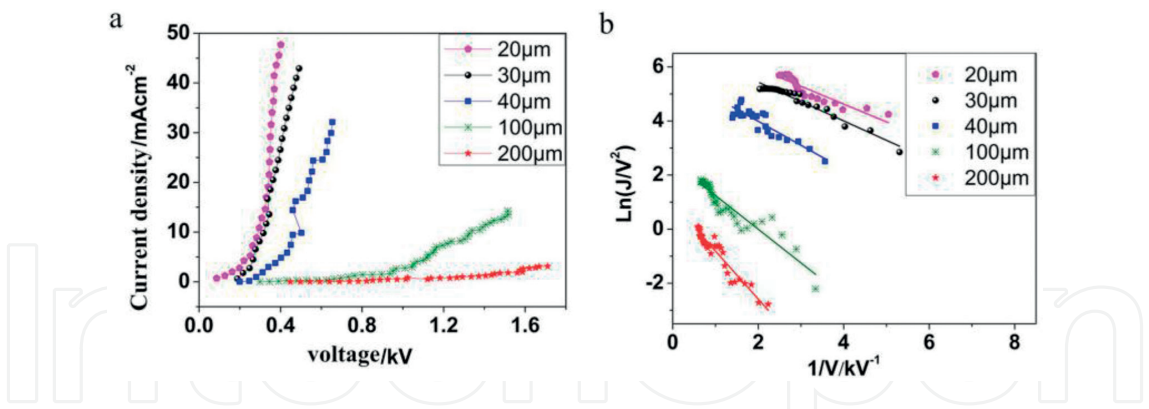
Figure 10. Field emission results of CNT arrays covered on fibers surfaces with diameters of 20, 30, 40, 100, and 200 μm. (a) *J-V* curve of emission current, (b) the F-N plots.

Diameter (μm)	20	30	40	100	200
V_{to}	109	190	270	730	1290
β	11.631	11.338	10.562	9247	7823

Table 1. The turn-on voltage (V_{to}) and the field enhancement factor (β) of CNTs cathodes covered on fibers surfaces with diameters of 20, 30, 40, 100, and 200 μm.

β of the emitter and result in a high V_{to} and small emission current, which is a defect for field emission. Thus, β is greatly dependent on the surface morphology of cathodes. The method of growing CNT arrays on fiber surface is efficient and feasible to tuning β by fiber diameter. With the fiber diameter decreasing, the gaps of tips enlarge and β increase subsequently because of weakening screening effect of CNT emitters. [14]. To illustrate the screening effect on the tips of CNT arrays, a simple electrostatic simulation is carried out by commercial software (Comsol 3.5a, emes mode of AC/DC Module). **Figure 11** shows the simulation results, performing equipotential lines of the electrostatic field near CNT
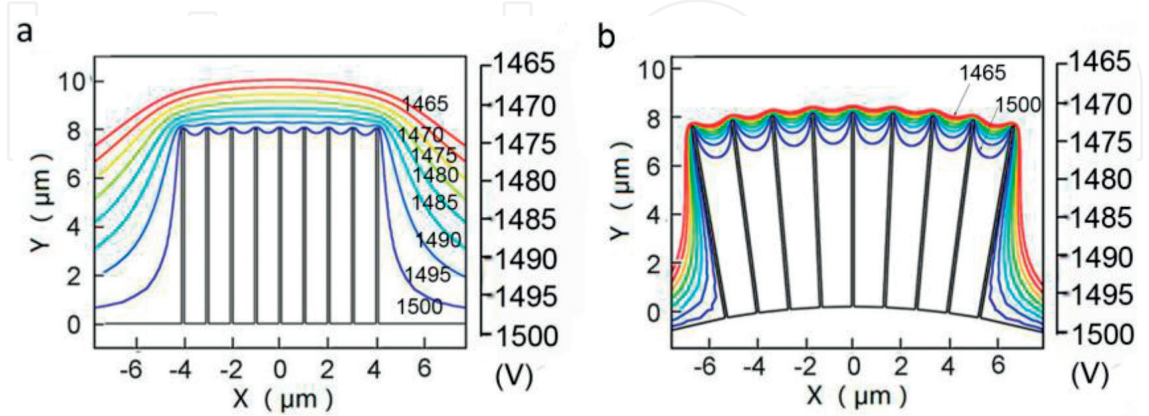

Figure 11. Simulation potential lines of the electric field near CNTs tips on a surface with diameter (Comsol 3.5a, emes mode of AC/DC module). (a) 200 μm, and (b) 20 μm, respectively. The unit in color bar is volt. The color bar ranges from −1500 to −1465 V.

tips on fiber substrates, a circular curving surface with curvature radius 200 and 20 μm, as shown in **Figure 11(a)** and **(b)**, respectively. With the curvature radius of substrate reduce, the spacing and the density of the equipotential lines on tips surface increase. This result demonstrates the decreased screening effect of the CNT arrays that lies on a smaller diameter fiber substrate.

4. Laser-induced field emission

Laser-induced field emission could offer opportunities for dramatic improvements in performance of electronic devices due to the possibility of manipulation and control of coherent electron motion in ultrafast spatiotemporal scales [8, 21]. As one of the most important cold cathode materials, CNTs have been widely studied. Synthesis of well-aligned CNTs on substrates of various geometries is also of special interest to the exploration of laser-induced field emission. Here, CNT arrays on fiber substrate serve as an emitter to explore the mechanism of laser-induced field emission.

From Eq.(1), we know that enhancing β or decreasing φ can improve field emission properties. As for a given material for cathode, φ is a constant. Generally, enhancing β by changing the tip morphology of the emitters is one of the main strategies. Herein, the improvement of field emission can be attributed to decreasing φ of CNT arrays because of the photon absorption. In this part, it will take advantage of laser leakage from an optical fiber to illuminate the cathode for realizing laser-induced field emission.

The cathode of laser-induced field emission is the CNT arrays emitters, which cover on the fiber substrate, as reported in **Figure 6**. **Figure 12** shows the schematic diagram of laser-induced field emission measurement set-up for the cathode of CNT arrays on an optical fiber.

The field emission properties of the cathode are measured in two cases: with laser-on and laser-off. **Figure 13(a)** shows the measurement results of the CNT arrays cathodes on optical fiber with the diameter of 30 μm. The turn-on voltage (a voltage requires an emission current density reaching to 1 mA·cm^{-2}) of laser-on state is 0.89 kV ($V_{\text{to-on}}$), and 1.01 kV ($V_{\text{to-off}}$) on laser-off state. $V_{\text{to-on}}$ is much lower than $V_{\text{to-off}}$. Besides, emission current on laser-on state is enhanced comparing with emission current on laser-off state. At 1 kV bias voltage, the emission current density on laser-on state ($J_{\text{E-on}}$) is 3.78 mA·cm^{-2} while 1.10 mA·cm^{-2} on laser-off state ($J_{\text{E-off}}$). The field emission properties on laser-on state are better than that of properties on laser-off state, as shown in **Figure 13(b)** and **(c)**. **Figure 13(b)** shows the emission current of CNT arrays on fiber diameter of 40 μm on laser-on and laser-off state. **Figure 13(c)** is the field emission results on fiber diameter of 140 μm.

As mentioned above, β and φ of the cathode are two critical factors for the field emission properties. β strongly depends on the cathode morphology. For a given optical fiber substrate, β keeps constant whenever CNT is on laser-on or laser-off states. Thus, the enhanced emission property is attributed to effective φ decreased by photon absorption. As shown in
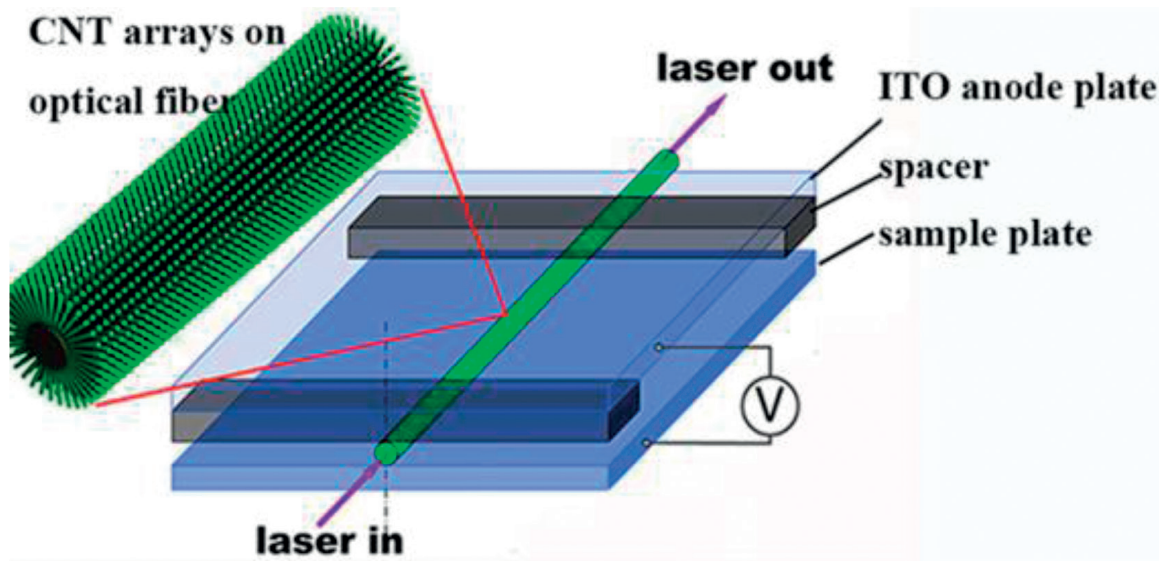
Figure 12. Schematic of laser-induced field emission measurement set-up.

Figure 13(a), when the fiber diameter fixed at 30 μm, β of the CNT arrays cathode is a constant of 4.89 eV. However, the turn-on voltage and emission current density are modulated by introducing laser into the optical fiber. The enhanced property is evaluated by measuring $\Delta\varphi$. According to the F-N plot and Eq.(1), the value of the effectiveφ, $\Delta\varphi_{'}$ and β are deduced and listed in **Table 2**. β of the cathode on the optical fiber with diameter of 30 μm is 4672, while that of the cathode on the fiber with diameter of 40 and 140 μm is 2804 and 2526. The different β is attributed to the different curvature of the cathode on fibers with different diameters, agreeing with the above discussion. What we are concerned here is the change of the work function $\Delta\varphi$of the cathode causing by the laser field. From **Table 2**, the work function significantly reduces to 4.14 eV when the fiber substrate diameter is 30 μm on the laser-on state. While the cathodes on fibers with diameters of 40 and 140 μm, the work function reduce to 4.28 and 4.76 eV, respectively.
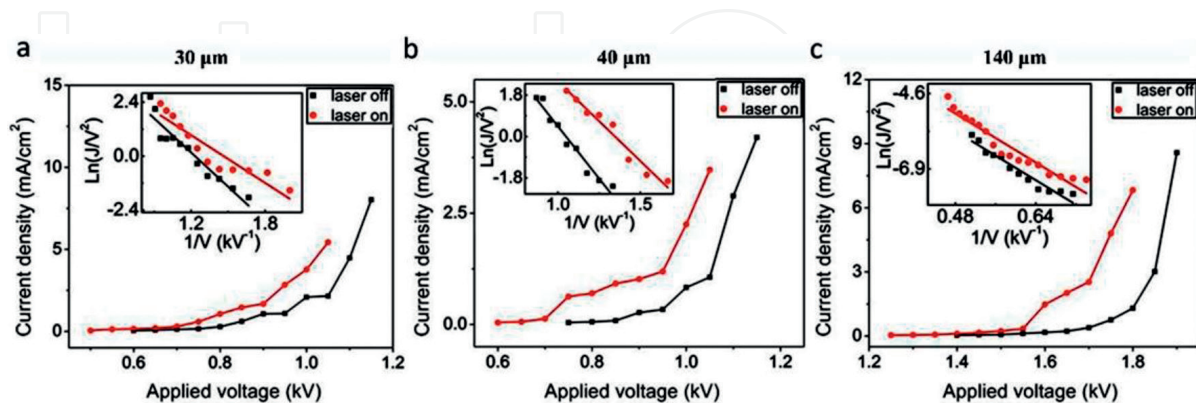

Figure 13. Laser-induced field emission measurement results. (a) The emission current density versus applied field voltage (*J-V*) curves of cathode of CNT arrays on optic fiber with the diameter of 30 μm on laser-on and laser-off cases. Inset is the corresponding F-N plot. (b) Fiber diameter is 40 μm. (c) Fiber diameter is 140 μm.

Diameter	30 μm	40 μm	140 μm
$\varphi_{\text{laser-on}}$	4.14 eV	4.28 eV	4.76 eV
$\Delta\varphi$	0.74	0.49	0.12
β	4672	2804	2526

Table 2. The effective work function φ, $\Delta\varphi=|\varphi_{\text{laser-on}}-\varphi_{\text{laser-off}}|$, and the field enhancement factor β of CNT arrays on fibers substrate with the diameter of 30, 40, and 140 μm on both laser on and off state.

The key factor of influencing φ is the laser field. On the laser-on state, the leakage of laser from the fiber surface is absorbed by CNT cathodes, when laser propagate through the fiber substrate. The electrons are excited to high-energy states and then emit to vacuum on applied voltages. So, the effective work function φ of CNT cathodes should subtract $\Delta\varphi$ (arise from absorbing photons) from 4.89 eV for laser-induced field emission. These results open a new way to improve field emission properties by the work function of cathodes and provide a preparation for realizing pulsed field emission.

5. Pulsed field emission

Illuminating a sharp cathode tip with laser pulses leads to pulsed field emission. A number of studies clarified the intriguing characteristics of the electron emission processes. This part explores pulsed field emission from CNT cathodes.

As mentioned above, the field emission property was modulated by optical field using a continuous wave laser (CW laser) in the laser-induced field emission. Electrons pump up a high-energy state by laser illumination and then tunnel through barrier to emit into vacuum. The emission current is closely related to CW laser field. So, the CW laser is replaced by pulsed laser to desire a discontinuous modulated signal of pulsed emission current. Herein, the pulsed field emission is based on laser-induced field emission. Illuminating CNT arrays with infrared laser pulses leads to pulsed field emission. **Figure 14(a)** shows the experimental set-up of pulsed field emission from CNT cathodes on Si substrate. **Figure 14(b)** shows the
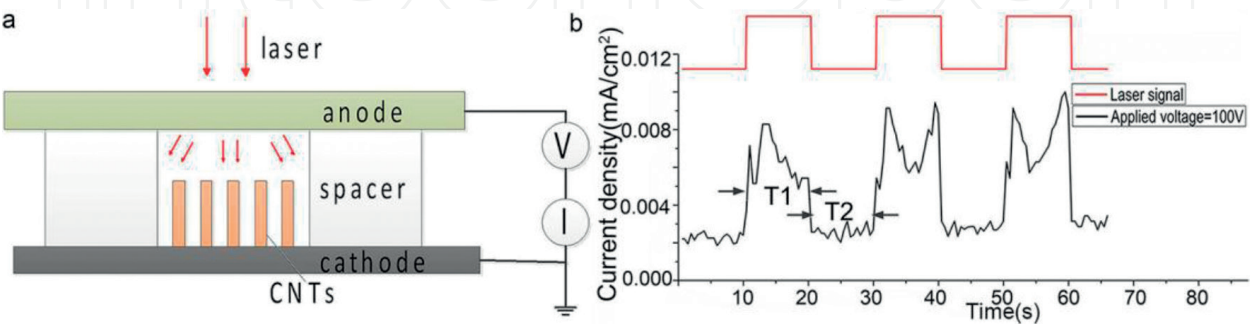

Figure 14. (a) Experimental set-up of pulsed field emission. (b) Electronic pulses from CNT cathodes illuminated by pulsed laser, on applied voltage of 600 V. Laser pulse-on and laser pulse-off are both 10000 ms.

pulsed emission current from CNT cathodes, when the pulse width (Pulse-on denotes the pulse duration expressing by T1) and the trough width (Pulse-off denotes time interval of two pulses expressing by T2) are both 10,000 ms. Importantly, the emission electronic pulses is almost synchronous with laser pulses with the electronic pulse duration of 10,000 ms or so, proving that electron emissions are intensively depended on the condition of laser pulse-on (T1). The average peak value of emission pulses density is 0.0068 mA/cm² with a little fluctuation on applied voltage of 600 V. The results demonstrate the realization of emission pulses from CNT cathodes. Besides, the field emission current density is about 0.0023 mA/cm² on laser pulse-off, which is much less than the emission current on laser pulse-on. It can be said the emission current can be enhanced by laser field.

Figure 15 shows emission pulses of pulsed field emission from CNT emitters illuminated by laser pulses, on the applied voltage of 100, 300, 500, 700, 900, and 1000 V with the same laser work condition. Increasing applied voltage, the peak value of emission pulses markedly increases on low applied voltage, as shown in **Figure 15(a)–(c)**. Although the peak value of emission pulses increase with the continually increasing applied voltage, the emission pulses trend to decrease on high applied voltage, as shown in **Figure 15(d)–(f)**. **Table 3** demonstrates values of the ratio of $\eta = I_{on}/I_{off}$ on different applied voltage. I_{on} is the average peak value of emission pulses density on pulse-on, and I_{off} is the average trough value of emission current density on pulse-off. The emission pulses are visible on low applied voltages, but the pulses cannot be distinguished on the high voltage of 1000 V ($\eta \approx 1$, that is $I_{on} \approx I_{off}$).
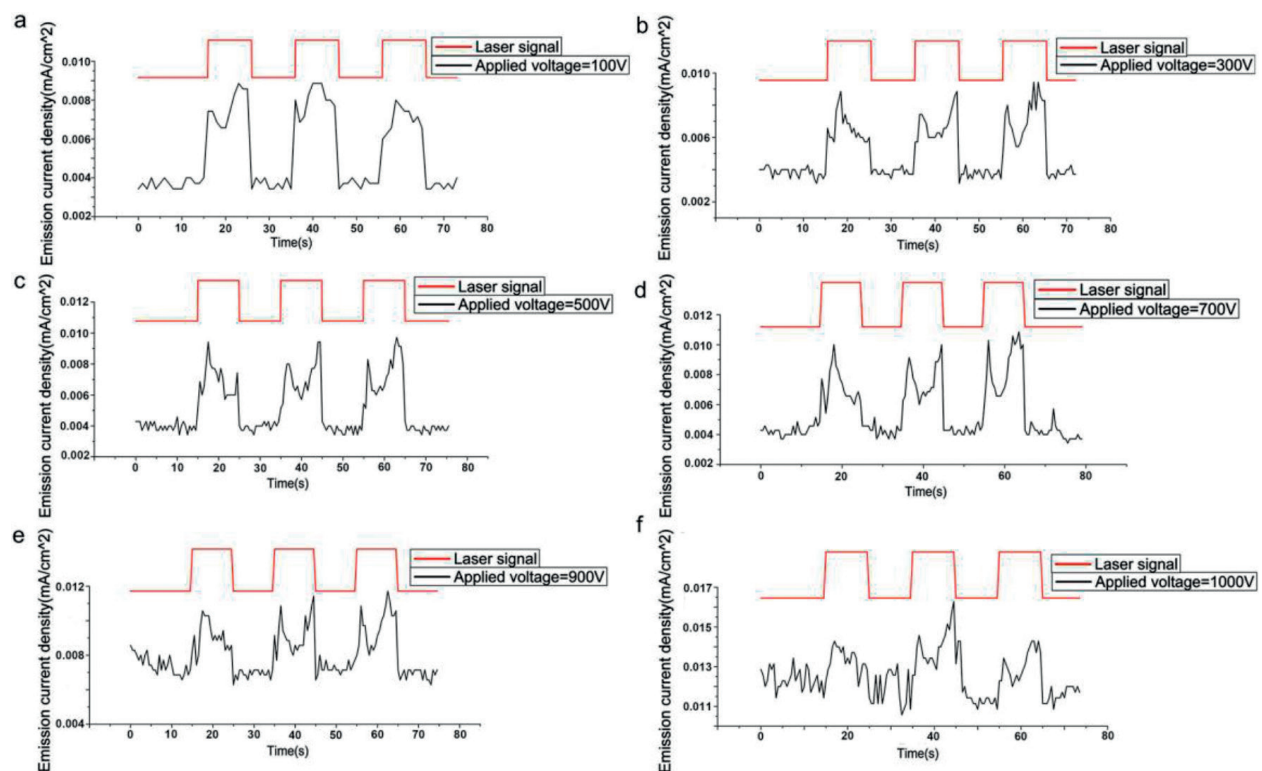

Figure 15. Electronic pulses of pulsed field emission from CNT cathodes illuminated by the same pulsed laser, but on the different applied voltage. Laser pulse-on (T1) and laser pulse-off (T2) are both 10000 ms. (a) on applied voltage of 500 V, (b) 600 V, (c) 700 V, and (d) 800 V.

Voltage (V)	100	200	300	400	500	600	700	800	900	1000
Ratio (mA/cm^2) I_{on}/I_{off}	2.09	2.48	3.53	4.07	5.07	2.09	1.98	1.55	1.39	≈1

I_{on} is the average peak value of emission electronic pulses density on pulse-on, and I_{off} is the average trough value of emission current density on electron pulse-off.

Table 3. The ratio values of $\eta = I_{on}/I_{off}$ on different applied voltage of 100, 200, 300, 400, 500, 600, 700, 800, 900, and 1000 V.
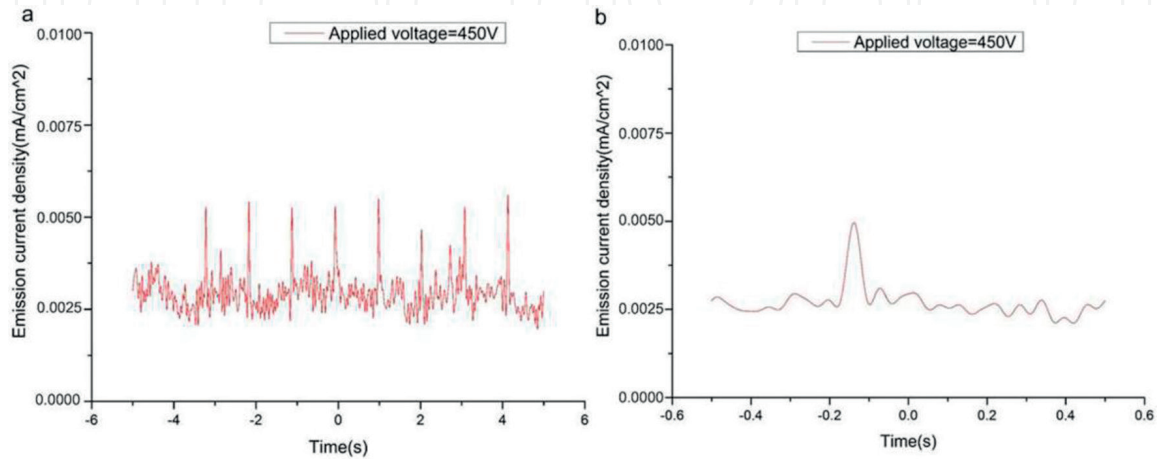

Figure 16. Electronic pulses with width of 50 ms from CNT arrays cathode on applied voltage of 450 V. (a) T1 = 50 ms, T2 = 1000 ms. (b) the detailed information of an electronic pulse.

In fact, emission mechanism is dominated by the electric field on high voltages, while laser field does not play an important role in the emission process. As the applied voltage continuously increases, emission electrons induced by laser pulses can be ignored due to it is too weak comparing with emission current of the field emission, just leading to a fluctuation for emission current. So, the pulsed field emission happens on the low applied voltage, and is greatly depending on the laser pulses. The results explain the emission mechanism and pave a way for realizing pulsed field emission from CNT cathodes.

Shortening the pulse cycle is a conventional method in order to increase the frequency of emission pulses for pulsed field emission. We try to decrease the pulse width to study short electronic pulses from pulsed field emission of CNT cathodes. **Figure 16** shows emission pulses of 50 ms from CNT emitters, on the laser work condition of T1 = 50 ms and T2 = 1000 ms. The results show the width and the time pulse-off of emission pulse is 50 and 1000 ms, synchronously with the laser pulse train. **Figure 16(b)** is the detailed information about an electronic pulse of 50 ms.

However, there is an inevitable problem of thermal effect existing in the pulsed field emission. Laser illumination makes CNT emitters heat up and causes a thermal effect during the emission process. For the further information of the thermal effect, we detect the response time of electronic pulses by oscilloscope with sampling rate of 2.5 GS/s. The results show that the electron emission is not instantaneous with the laser field. The rise and fall time spend more than 2 s on laser pulse-on and pulse-off, as shown in **Figure 17**. Generally, the thermal effect will lead to a response time, but the field emission is instantaneous. For the pulsed field emission, the response time and pulse broadening are the weaknesses causing by thermal effect. Especially, in the short emission electronic pulses, pulse broadening limits the possibility of
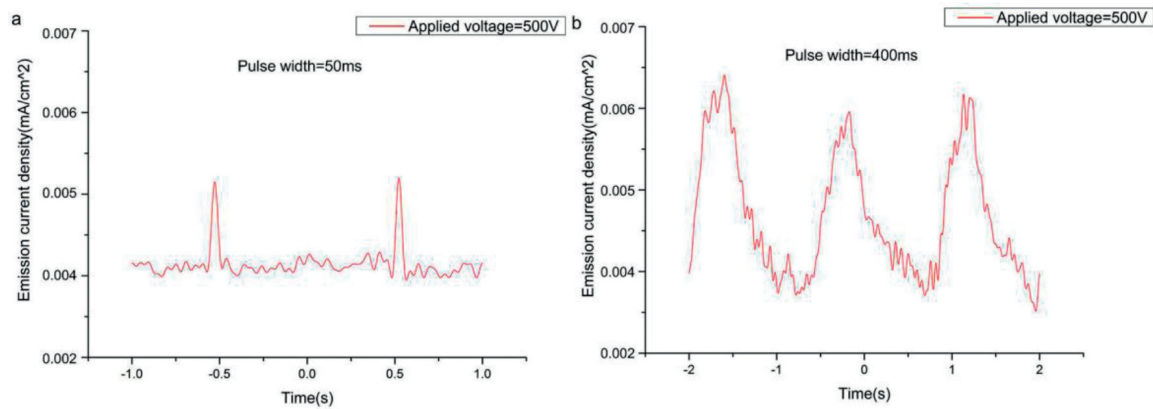
Figure 17. Electronic pulses with width from CNT arrays cathode on applied voltage of 500 V. (a) T1 = 50 ms, T2 = 1000 ms. (b) T1 = 400 ms, T2 = 1000 ms.

the high frequency and short pulse because of the thermal effect, as shown in **Figure 17(b)**. Nevertheless, there is an advantage of enhancing emission current for thermal effect in the pulsed field emission. As shown in **Figure 17**, the peak value of the electronic pulses is quite different on the same work condition but different T1. For **Figure 17(b)**, the emission current is compelled drop down before reach to the peak value of 0.006 mA/cm^2 comparing with **Figure 17(a)**. With the T1 increase, the emission current is enhanced resulting from thermal effect, which is beneficial for the pulsed field emission.

These results show that thermal effect enhances the pulsed field emission of CNT cathodes illuminating by pulsed laser, but emitting short electronic pulses are strongly influenced by thermal effect resulting in pulse broadening. So, the optimum work condition of laser pulse is T2 ≥ T1 for pulsed field emission, especially in realizing ultrashort electronic pulses. It provides a preparation for us studying ultrafast electron source.

Acknowledgements

Author details

Xianqi Wei[1,2,3*]

*Address all correspondence to: wei.wxq@163.com

1 Science School, HuaiHai Institute of Technology, Lianyungang, Jiangsu, China

2 Department of Microelectronics, School of Electronics and Information Engineering, Xi'an Jiaotong University, Xi'an, Shaanxi, China

3 Research Institute of Xi'an Jiaotong University, Hangzhou City, Zhejiang Province, China

References

[1]   Nojeh A. Carbon nanotube electron sources: From electron beams to energy conversion and optophononics. ISRN Nanomaterials. 2014;**2014**(1):879827-879851. DOI: 10.1155/2014/879827

[2]   Tian S, Li H, Zhang Y, Liu S, Fu Y. Potential field emitters: HfC nanorods sheathed with a HfO$_2$ nanoshell. CrystEngComm. 2014;**16**(15):3186-3191. DOI: 10.1039/c3ce42478b

[3]   Xu NS, Huq SE. Novel cold cathode materials and applications. Materials Science & Engineering R. 2005;**48**(2-5):47-189. DOI: 10.1016/j.mser.2004.12.001

[4]   Wei XQ, Li X, Liu WH, Wang XL. Laser tuned field emission of the car bon nanotube arrays grown on an optical fiber. Science China Technological Sciences. 2014;**57**(10):1936-1940. DOI: 10.1007/s11431-014-5630-1

[5]   Krüger M, Schenk M, Hommelhoff P. Attosecond control of electrons emitted from a nanoscale metal tip. Nature. 2011;**475**(7354):78-81. DOI: 1038/nature10196

[6]   Vogelsang J, Robin J, Nagy BJ, Dombi P, Rosenkranz D, Schiek M, Grob P, Lienau C. Ultrafast electron emission from a sharp metal nanotaper driven by adiabatic nanofocusing of surface plasmons. Nano Letters. 2015;**15**(7):4685-4691. DOI: 10.1021/acs.nanolett.5b01513

[7]   Zhang P, Lau YY. Ultrafast strong-field photoelectron emission from biased metal surfaces: Exact solution to time-dependent Schrödinger equation. Scientific Reports. 2016;**6**:19894-19906. DOI: 10.1038/srep19894

[8]   Lyashenko DA, Svirko YP, Petrov MI, Obraztsov AN. The laser assisted field electron emission from carbon nanostructure. Journal of the European Optical Society-Rapid Publications. 2017;**13**(1):4-10. DOI: 10.1186/s41476-017-0033-0

[9]   Krüger M, Schenk M, Förster M, Hommelhoff P. Attosecond physics in photoemission from a metal nanotip. Journal of Physics B Atomic Molecular & Optical Physics. 2012;**45**(7):074006-074012. DOI: 10.1088/0953-4075/45/7/074006

[10] Zhang L, Zhang HMDPI. A survey on security and privacy in emerging sensor networks: From viewpoint of close-loop. Sensors. 2016;**16**(4):443-459. DOI: 10.3390/s16040443

[11] Deng JH, Zheng RT, Yang YM, Zhao Y, Cheng GA. Excellent field emission characteristics from few-layer graphene–carbon nanotube hybrids synthesized using radio frequency hydrogen plasma sputtering deposition. Carbon. 2012;**50**(12):4732-4737. DOI: 10.1016/j.carbon.2012.05.065

[12] Chen F, Ji X, Zhang Q. Radial AlN nanotips on carbon fibers as flexible electron emitters. Carbon. 2015;**81**:124-131. DOI: 10.1016/j.carbon.2014.09.037

[13] Kanth SK, Sharma A, Park BC, Kim HS. Multiwalled carbon nanotube field emitter as an electron source for a microcolumn. Journal of Vacuum Science & Technology B. 2016;**34**(1):011805-011811. DOI: 10.1116/1.4939834

[14] Wei X, Zhu Y, Xia X, Wang X, Liu W, Xin L. Carbon nanotube cathodes covered on the cylindrical surface of a fiber. RSC Advances. 2015;**5**(22):17049-17053. DOI: 10.1039/C4RA14537B

[15] Shao X, Srinivasan A, Zhao Y, Khursheed A. A few-layer graphene ring-cathode field emitter for focused electron/ion beam applications. Carbon. 2016;**110**:378-383. DOI: 10.1016/j.carbon.2016.09.048

[16] Xu S, Rezvanian O, Kara P, Zikry MA. Tunneling effects and electrical conductivity of CNT polymer composites. MRS Online Proceedings Library (OPL). 2011;**1304**:6697-6718. DOI: 10.1557/opl.2011.606

[17] Lei W, Zhu Z, Liu C, Zhang X, Wang B, Nathan A. High-current field-emission of carbon nanotubes and its application as a fast-imaging X-ray source. Carbon. 2015;**94**:687-693. DOI: 10.1016/j.carbon.2015.07.044

[18] Wimalasiri Y, Zou L. Carbon nanotube/graphene composite for enhanced capacitive deionization performance. Carbon. 2013;**59**(7):464-471. DOI: 10.1016/j.carbon.2013.03.040

[19] Zhao N, Chen J, Qu K, Khan Q, Zhang X. Stable electron field emission from carbon nanotubes emitter transferred on graphene films. Physica E: Low-Dimensional Systems and Nanostructures. 2015;**72**:84-88. DOI: 10.1016/j.physe.2015.04.024

[20] Deng JH, Zheng RT, Zhao Y, Cheng G. Vapor-solid growth of few-layer graphene using radio frequency sputtering deposition and its application on field emission. ACS Nano. 2012;**6**(5):3727-3733. DOI: 10.1021/nn300900v

[21] Bionta M, Chalopin B, Delmas M, Chatel B. Ultrafast laser-induced field emission from a single carbon nanotube based nanotip. In: Lasers and Electro-Optics (CLEO); 10-15 May 2015; San Jose. USA: IEEE; 2015. pp. 1-2